# Photoinduced Energy Shift in Quantum-Dot-Sensitized TiO2: A First-Principles Analysis

**ARTICLE** *in* JOURNAL OF PHYSICAL CHEMISTRY LETTERS · MARCH 2015

Impact Factor: 7.46 · DOI: 10.1021/acs.jpclett.5b00393



**3 AUTHORS:**

Jon Mikel Azpiroz
Italian National Research Council
**21** PUBLICATIONS **142** CITATIONS
SEE PROFILE

Enrico Ronca
Princeton University
**16** PUBLICATIONS **386** CITATIONS
SEE PROFILE

Filippo De Angelis
Università degli Studi di Perugia
**265** PUBLICATIONS **11,207** CITATIONS
SEE PROFILE

THE JOURNAL OF PHYSICAL CHEMISTRY Letters

Letter

pubs.acs.org/JPCL

# Photoinduced Energy Shift in Quantum-Dot-Sensitized $TiO_2$: A First-Principles Analysis

Jon M. Azpiroz,*[,†,‡] Enrico Ronca,[†] and Filippo De Angelis*[,†]

[†]Computational Laboratory for Hybrid/Organic Photovoltaics (CLHYO), Istituto CNR di Scienze e Tecnologie Molecolari (CNR-ISTM), Via Elce di Sotto 8, 06123 Perugia, Italy

[‡]Kimika Fakultatea, Euskal Herriko Unibertsitatea (UPV/EHU) and Donostia International Physics Center (DIPC), P. K. 1072, 20080 Donostia, Euskadi, Spain

Supporting Information

**ABSTRACT:** We investigate the photoinduced dipole (PID) phenomenon, which holds enormous potential for the optimization of quantum dot-sensitized solar cells (QDSSCs), by means of first-principles electronic structure calculations. We demonstrate that the sensitization of the $TiO_2$ substrate with core/shell QDs produces almost no changes in the ground state but decisively improves the performance upon photoexcitation. In particular, the maximum attainable $V_{OC}$ is predicted to increase by ∼25 meV due to two additive effects: (i) the displacement of the photoexcited hole away from the $TiO_2$ surface and (ii) the interfacial electrostatic interaction established between the $TiO_2$-injected electrons and the holes residing in the QD core. We believe that this work, explaining the mechanisms by which PID cells deliver better efficiencies, paves the way for the design of new QDSSCs with improved efficiencies.

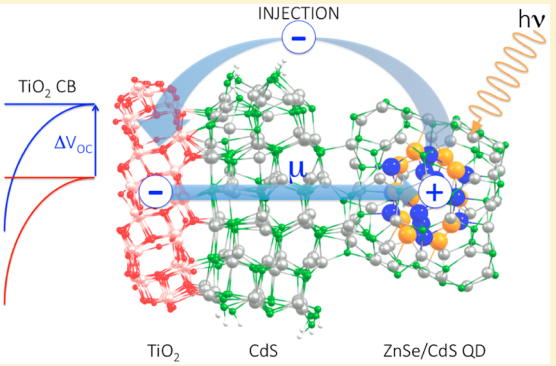


Semiconductor quantum dots (QDs)[1,2] have attracted a great deal of research due to their outstanding optoelectronic properties, including their intrinsically large extinction coefficients and their size- and shape-dependent electronic structure, which make them particularly amenable for sensitization.[3] The tunability of the electronic levels is particularly important because it provides an elegant means to adjust the optical features of the QDs in such a way that a better overlap with the sunlight is achieved. Moreover, the on purpose modification of the band edges could promote interfacial charge-transfer processes in QD-sensitized solar cells (QDSSCs) due to a favorable alignment of the electronic levels with respect to other components of the solar device. Besides, QDs provide the opportunity to increase cell photocurrent by either extracting hot carriers or taking advantage of the multiple exciton generation (MEG) phenomenon,[4,5] which can potentially overcome the Shockley−Queisser limit of 33% power conversion efficiency (PCE).[6] The operational mechanism of QDSSCs[7−10] is similar to their dye-based counterparts (DSSCs).[11] In brief, QDs absorb solar radiation and inject the photoexcited electrons into the conduction band (CB) of a wide-band-gap semiconductor (usually $TiO_2$), while the concomitant holes are transferred to a redox mediator (typically $S^{2-}/S_x^{2-}$).

QDSSCs have performed quite disappointingly so far, with record efficiencies of 7%,[12] far below their dye (13%)[13] and perovskite (19%)[14,15] sensitized analogues. Many reasons have been put forward to explain such poor performance,[7−10] including the intrinsically low photovoltage due to the highly negative redox potential of the commonly used polysulfide electrolyte. To overcome this drawback, alternative mediators with more positive redox potentials are being explored, including the cobalt-based ones[16] or solid-state hole conductors, such as spiro-OMeTAD or P3HT.[17−21]

A different route for improving the voltage of QDSSCs implies the use of organic additives, which adsorbed on $TiO_2$ modifies its electronic properties. In particular, molecules with a dipole moment pointing away from the $TiO_2$ surface have been found to negatively shift the CB edge of the oxide, increasing the $V_{OC}$ and therefore improving the performance of the device.[22,23] Notably, the shift of the $TiO_2$ unoccupied levels correlates linearly with the coverage and the dipole component normal to the oxide surface. A similar manipulation of the QD energy levels has been achieved by adsorbing benzenethiol and acid derivative molecules with different molecular dipole moments.[24−26] Therefore, polar surfactants may allow fine engineering of the interfacial electronic levels in QDSSCs. However, the impact of the adsorbed molecules on the electronic levels of both the QD sensitizer and the oxide substrate is quite small because the dipoles at the interface are based on partial charges.

**Received:** February 23, 2015
**Accepted:** March 31, 2015





DOI: 10.1021/acs.jpclett.5b00393
J. Phys. Chem. Lett. 2015, 6, 1423−1429

QD sensitizers have been shown to build up a chemical potential by themselves upon illumination, most likely due to accumulation of photogenerated charges in surface trap states.[7,27] Control over this kind of photoinduced phenomena, which contributes to the total chemical capacitance in QDSSCs, could pave the way for the on purpose modification of the energy level alignment of the system while gaining extra photovoltage. Inspired by this idea, multilayer QD organizations have been proven to improve the performance of QDSSCs.[28]

More recently, a novel configuration of QDSSCs has been developed, which is rooted on the photoinduced dipole (PID) phenomenon.[29,30] This new realization is based on type-II core/shell QDs, which are characterized by a staggered band alignment of the electronic levels, with the valence band (VB) and the CB edges being located in the core and the shell materials, respectively. Upon illumination, the photoexcited electrons spread over the shell region, whereas the holes remain confined in the core. In Figure 1a, the working mechanisms of

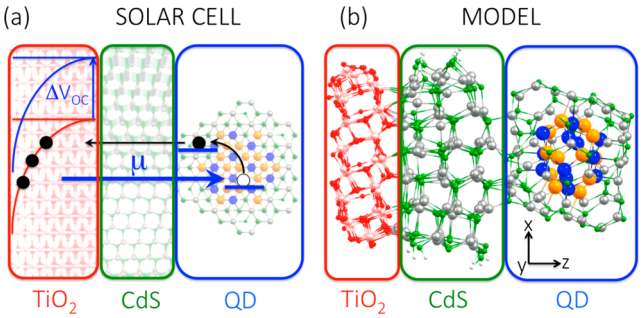


**Figure 1.** (a) Schematic representation of the functioning of the PID QDSSC. (b) Optimized structure of the model employed to represent the PID cell. Pink = Ti, red = O, gray = Cd, green = S, white = H, blue = Zn, and orange = Se atoms.

the PID device are depicted, which following the seminal work by Zaban et al.,[30] comprises (i) a $TiO_2$ oxide substrate, (ii) a CdS layer, and (iii) a ZnSe/CdS core/shell QD. Upon photoexcitation, the core/shell QDs inject electrons into the manifold of $TiO_2$ unoccupied states. The electron injection leaves long-lived holes in the QD core, which are regenerated by the electrolyte on a time scale of several hundred $\mu$s.[29] The hole extraction is therefore slow enough to allow the development of a large dipole between the newly injected electrons and the holes confined in the sensitizer, resulting in an improvement of ~100 mV in the photovoltage; see Figure 1a.[30] Such an unprecedented increase of the $V_{OC}$ has been attributed to the large electrostatic effect induced by the photogenerated charges.

In this Letter, we report on the computational modeling of the energy shifts possibly underlying the PID phenomenon, which holds enormous potential for the optimization of QD-based solar cell devices. On the basis of density functional theory calculations (see the Computational Details section below), we demonstrate that the incorporation of core/shell QDs into standard QDSSCs produces almost no changes in the ground state (GS) but decisively improves the performance of the cell upon photoexcitation. In particular, the maximum attainable $V_{OC}$ is predicted to increase by ~25 meV due to two additive effects: (i) the displacement of the photoexcited hole away from the $TiO_2$ surface and (ii) the interfacial electrostatic interaction established between the $TiO_2$-injected electrons and the holes residing in the QD core.

In Figure 1b, we depict the optimized geometry of the model used for the simulation of the solar device. To properly reproduce the relevant interfaces lying at the heart of QDSSCs, it is crucial to choose realistic models for the individual components. Therefore, to simulate the metal oxide, a 2.0 × 2.0 × 0.5 nm size $(TiO_2)_{82}$ slab exposing a majority of (101) surface has been sliced from the underlying anatase crystal structure.[31] With a calculated optical gap of 3.4 eV, it fairly reproduces the absorption onset of the $TiO_2$ nanoparticles used in current solar devices.[32] Moreover, the position of the CB, ca. −3.8 eV, is in nice agreement with the experiments.[32]

To represent the CdS film, a 1 nm thick $(CdS)_{93}$ cluster of wurtzite structure has been built up, which exposes a majority of apolar (1010) facets, as found experimentally for most of the II−VI semiconductor nanostructures.[33] Following our previous computational works in this kind of clusters,[34,35] the Cd- and S-terminated (0001) surfaces have been capped with $HS^-$ and $H^+$ ions, in order to saturate the dangling atoms and avoid the development of a fictitious dipole along the CdS layer, which would otherwise give rise to a spurious shrinkage of the band gap. Accordingly, our passivated CdS cluster exhibits a HOMO−LUMO gap of 2.6 eV, calculated at the geometry that it adopts in the interacting cell model, see Figure 1b, in nice agreement with the experimental absorption onset of similarly small nanostructures (~2.8 eV).[36]

Finally, to simulate the core/shell QD, we built up a 1.5 nm size spherical $(ZnSe)_{12}/(CdS)_{48}$ cluster, based on the $(ZnS)_{12}/(ZnS)_{48}$ cluster first reported by Hamad et al. as the lowest-lying isomer for the $(ZnS)_{60}$ stoichiometry.[37] With a computed band gap of 2.8 eV, our model is able to fairly reproduce the lowest optical feature of the core/shell QDs exploited in the actual solar cell, ~2.5 eV.[29] Furthermore, this new model captures the staggered alignment of the electronic levels of the type-II core/shell QDs employed experimentally. In Figure 2,

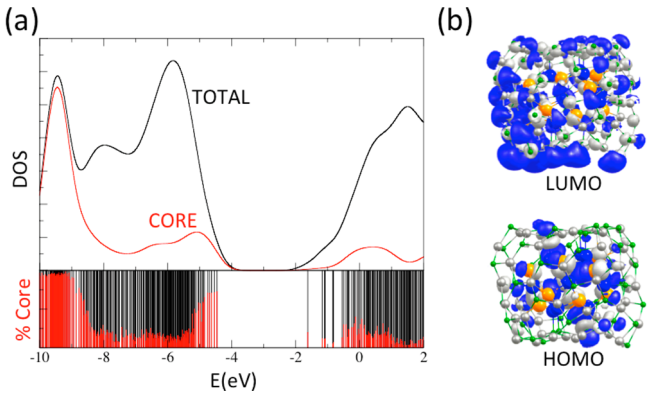


**Figure 2.** (a) DOS of the ZnSe/CdS QD, along with the projection DOS (PDOS) in the ZnSe core. (b) Isodensity plots of the highest occupied and the lowest unoccupied molecular orbitals (HOMO and LUMO).

the density of states (DOS) of the ZnSe/CdS QD is shown, along with the DOS projection in the ZnSe core. As is immediately clear, the CB states are mostly spread over the shell, whereas the highest occupied orbitals are located in the core. Upon illumination, the photoexcited electrons should localize in the CdS carapace, favoring electron injection due to the effective coupling with the oxide CB states. The


DOI: 10.1021/acs.jpclett.5b00393
J. Phys. Chem. Lett. 2015, 6, 1423−1429

concomitant holes, confined in the inner part of the QD, would then exert an electrostatic interaction across the device.

Experimentally, there are two main methodologies to couple the QD sensitizers and the $TiO_2$ substrate.[38] The in situ approaches, which include the chemical bath deposition (CBD) and the successive ionic layer adsorption and reaction (SILAR), imply the direct growth of the QD on the oxide surface. These techniques provide high surface coverage and direct connection between the cell constituents but suffer from poor control over the QD size, shape, and composition. Therefore, core/shell QDs are usually synthesized by means of colloidal techniques, which are conducted in organic solvents in the presence of coordinating ligands that dynamically adhere to the nanostructure surface and control the nucleation and growth processes. The native passivating molecules are often exchanged by water-compatible bifunctional linkers (i.e., mercaptopropionic acid, MPA), which assist the deposition of the QD on the $TiO_2$ substrate.

Experimentally, the CdS layer is grown on the $TiO_2$ substrate by means of the SILAR method on $TiO_2$,[30] as in our model. The core/shell QDs, in turn, are presynthesized and deposited on the substrate either via bifunctional linkers[12] or by means of the electrophoretic deposition (EPD) method.[30] For simplicity, we opted for the direct adsorption of the QDs, as in previous theoretical works.[39] Although ligand-capped QDs would probably better reproduce the experiment, this work aims at unraveling the energy shift due to the core/shell organization. Therefore, our bare models should capture in any case the experimental trends, even if they lack the surface molecules.

The interfaces are crucial in determining the electronic structure of solar cells. Therefore, upon first consideration, it is worth having a look at the two contact surfaces in the solar cell model, namely, $CdS/TiO_2$ and QD/CdS. At first glance of Figure 1b, the CdS film seems to perfectly match with the $TiO_2$ substrate. Upon interaction, a large number of Cd(CdS)−$O(TiO_2)$ and S(CdS)−$Ti(TiO_2)$ bonds are formed, as is evident from the radial distribution functions (RDFs) shown in Figure 3a. Moreover, both the Cd−O and the S−Ti RDFs are characterized by sharp features, even for large distances, meaning long-range ordering at the $CdS/TiO_2$ interface. The Cd−O bonds are particularly tight, with computed values of 2.15 Å. The Ti−S is slightly longer (2.47 Å) but short enough to allow chemical interactions.

Regarding the adsorption of the core/shell QD, the CdS layer seems to properly accommodate our ZnSe/CdS model, as shown by the Cd(QD)−S(CdS) and the S(QD)−Cd(CdS) RDFs, which again reveal a quite ordered interface. As a matter of fact, the QD shell and the CdS film share the same composition, even if the crystal structure is not identical. Nonetheless, the Cd−S bonds at the QD/CdS interface are slightly longer (2.55−2.58 A) than those inside of the QD (2.49 Å) or the CdS layer (2.52 Å), meaning a nonoptimal matching of the two components. The differences are however small and suggest quite a strong adsorption of the QD on the nanostructured film.

At this point, we focus on the electronic structure of the $QD/CdS/TiO_2$ interface. For comparison, we also consider the $CdS/TiO_2$ model, which represents a prototype of a standard cell. To avoid spurious effects that might come into play due to the geometrical relaxation, we calculate the electronic structure of $CdS/TiO_2$ at the $QD/CdS/TiO_2$ geometry. In Figure 4, the DOSs of both models are depicted, calculated for their GSs. For comparison, the DOSs of the freestanding fragments are also displayed.

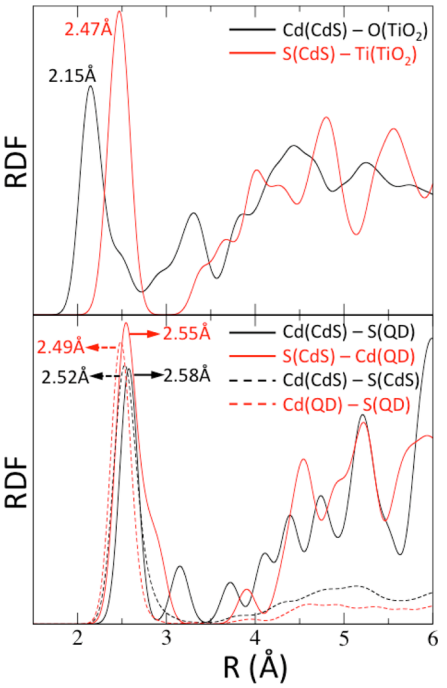


**Figure 3.** (a) Cd(CdS)−O (black) and S(CdS)−Ti (red) RDFs. (b) The same as in (a) but for Cd(CdS)−S(QD) (solid black) and S(CdS)−Cd(QD) (solid red). For comparison, the Cd(CdS)−S(CdS) (dashed black) and the Cd(QD)−S(QD) (dashed red) RDFs are also depicted.

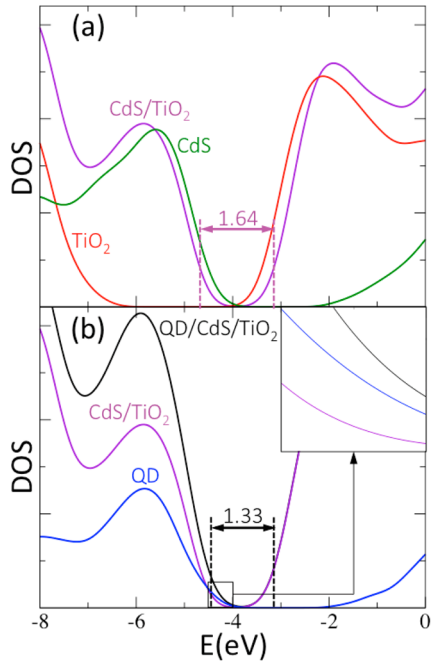


**Figure 4.** (a) DOS of the interacting $CdS/TiO_2$ system (purple), along with the DOS of the freestanding CdS (green) and $TiO_2$ (red) fragments. (b) DOS of the interacting $QD/CdS/TiO_2$ complex (black), along with the DOS of the freestanding $CdS/TiO_2$ (purple) and QD (blue) fragments. In the inset, a zoom of the VB edge region is shown.



DOI: 10.1021/acs.jpclett.5b00393
J. Phys. Chem. Lett. 2015, 6, 1423−1429

Regarding the standard cell model (see Figure 4a), the CdS occupied states intrude into the band gap of $TiO_2$, and the unoccupied states appear immersed in the manifold of the oxide conduction states. This kind of staggered alignment is a crucial prerequisite for the interfacial electron injection from the sensitizer film to the $TiO_2$ substrate. Interestingly, the VB and the CB edges are shifted by 0.15 and 0.20 eV with respect to the VB and the CB of the noninteracting CdS and $TiO_2$ fragments, respectively, suggesting that upon interaction, there is an important charge donation from the CdS sensitizing layer to the metal oxide substrate. In fact, the $TiO_2$ slab is predicted to bear a net charge of ~6 e in the interacting complex. This kind of polarization effects are similar to those characterized for molecular adsorbates and produce a comparable (upward) shift of the oxide CB edge, even in the GS. As one might notice from Figure 4b, the CB edge of the QD/CdS/$TiO_2$ coincides with the tail of unoccupied states of CdS/$TiO_2$, meaning that the oxide slab experience almost no change upon the adsorption of the core/shell QD on the CdS layer. The VB edge, instead, is shifted upward because the QDs introduce new states above the CdS HOMO (see the inset in Figure 4b). As a matter of fact, the HOMO of the QD/CdS/$TiO_2$ cell is mostly localized on the ZnSe/CdS QD.

To understand the photoinduced phenomena in this kind of photovoltaic systems, one has to move from the ground to the excited state. To this aim, we have calculated the lowest-lying triplet for the QD/CdS/$TiO_2$ model, which should fairly represent the charge-separated state (CSS). At first glance to the band alignment shown in Figure 4, photon absorption in the QD/CdS/$TiO_2$ cell should promote an electron from the QD (core) to the $TiO_2$ CB. This is clear from Figure 5a, where the spin density plot of the lowest-lying triplet state is shown.

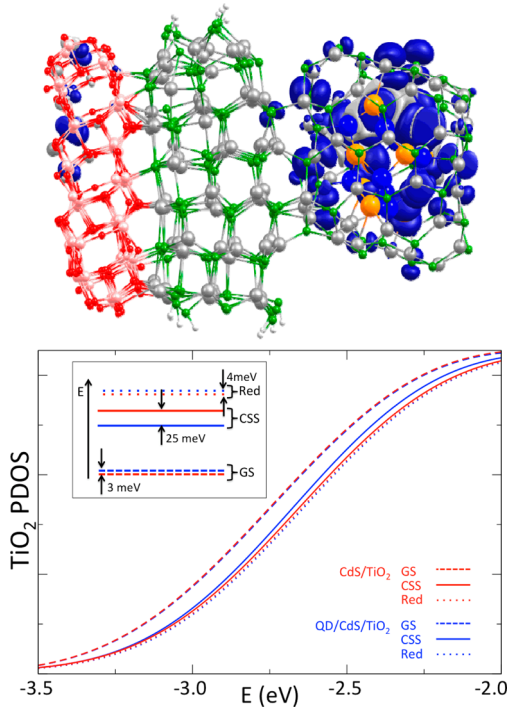


**Figure 5.** (Top) Spin density corresponding to the CSS of QD/CdS/$TiO_2$. (Bottom) CB edge, projected on the $TiO_2$ fragment, of the CdS/$TiO_2$ (red) and the QD/CdS/$TiO_2$ (blue) models, calculated for their GS (dashed lines), CSS (solid lines), and one-electron reduced states (Red, dotted lines).

Electron injection is further confirmed by the charge displacement analysis (CDA), which calculates the electron density difference between the CSS and the GS (for further details, see ref 22). According to CDA, upon photoexcitation, almost one electron is transferred from the QD core to the $TiO_2$ substrate; see the Supporting Information.

In Figure 5b, the CB edge of the QD/CdS/$TiO_2$ model is shown, calculated both for the GS and the CSS. For comparison, the corresponding DOSs of the CdS/$TiO_2$ system are also depicted. As is immediately clear, the standard and the PID cells share an almost identical CB edge in their GS. Upon photoexcitation, the CB edge experiences an upward shift in both systems, which is however more pronounced for the QD/CdS/$TiO_2$ system, as found in the experiments.[29,30] The computed difference between the standard and QD/CdS/$TiO_2$ cell models is 25 meV, in fair agreement with the experimental shift, which amounts to 70−100 meV, depending on the specific parameters of the device.[30] For completeness, we have also computed the one-electron reduced interface (Red), which represents the situation in which the photoexcited electron has been injected into $TiO_2$, and the concomitant hole has been compensated for by the redox couple. From Figure 5, the reduction of the CdS/$TiO_2$ and QD/CdS/$TiO_2$ systems further shifts the CB edge of the $TiO_2$ toward the vacuum due to the accumulation of negative charge in the oxide substrate. Similar to the neutral GS, however, the anionic complexes display a very similar CB tail, meaning that the better performance of the QD/CdS/$TiO_2$ cells is in fact a property related to the CSS.

Now, a question immediately arises: which is the exact physical phenomenon underlying the better performance of the QD/CdS/$TiO_2$ cell? From the experiments, the interfacial dipole has been claimed to be responsible for the improved efficiency of the modified device. However, one could also relate the CB shift in the QD/CdS/$TiO_2$ cell to two additional processes: (i) the accumulation of charge in the oxide, which shifts the $TiO_2$ unoccupied states upward, and (ii) the electrostatic potential generated by the photoexcited hole, which moves the CB edge downward. According to this picture, electron injection should produce a similar effect in both the standard and the QD/CdS/$TiO_2$ cell. In the QD/CdS/$TiO_2$ device, however, the positive charge lies far apart from the oxide surface, presumably producing a smaller shift of the oxide unoccupied states, which in turn leads to an improved $V_{OC}$. In the standard CdS/$TiO_2$ cell, the hole delocalizes over the CdS layer, quite close to the $TiO_2$ substrate, which experiences a strong (detrimental) electrostatic effect due to the positive charge.

To shed light on this issue, we have calculated the interfacial dipole moment along the $z$ axis of CdS/$TiO_2$ and QD/CdS/$TiO_2$; see the Supporting Information. According to the reference coordinate system depicted in Figure 1b, positive values of $\mu_z$ indicate that the dipole moment is pointing away from the $TiO_2$ slab, suggesting charge density concentration/depletion in the oxide substrate/QD sensitizer. As mentioned earlier, the adsorption of CdS on the $TiO_2$ slab comprises a charge donation from the sensitizer to the oxide slab of 6.0 e. Accordingly, a $\mu_z$ of +17 D is developed at the CdS/$TiO_2$ interface, which raises the oxide conduction states even in the GS. Electron injection induces a sizable reorganization of the electron density, which further increases the charge imbalance in the interacting system. In the CSS, the $TiO_2$ slab bears a negative charge of −6.8 e, and the interfacial $\mu_z$ amounts to +51 D, which further raises the $TiO_2$ CB. Regarding the QD/CdS/


DOI: 10.1021/acs.jpclett.5b00393
J. Phys. Chem. Lett. 2015, 6, 1423−1429

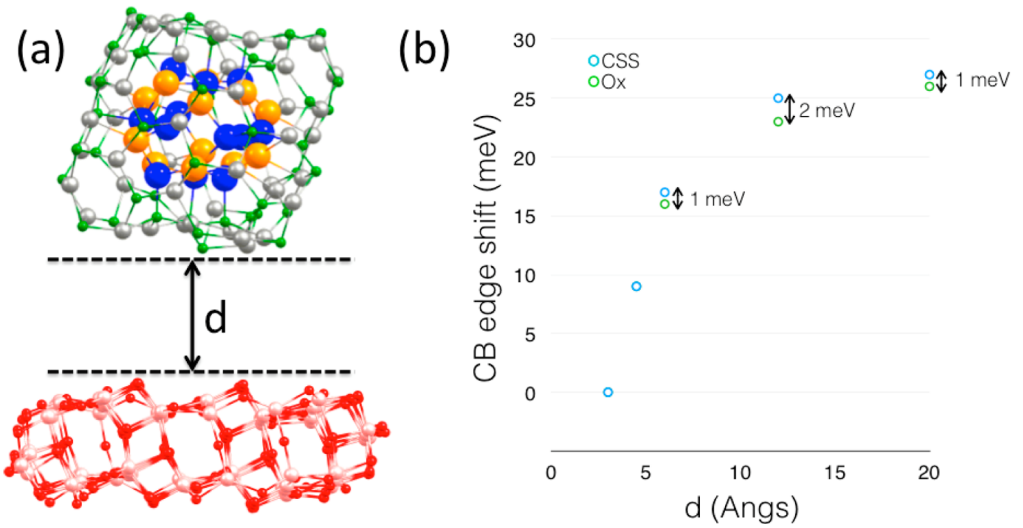


**Figure 6.** (a) Sketch of the QD/$TiO_2$ model. (b) CB edge of the QD/$TiO_2$ complex, calculated for different QD−$TiO_2$ distances ($d$ = 3.0, 4.5, 6.0, 12.0, and 20.0 Å), at their CSS (blue dots) and one-electron oxidized (Ox, green dots) electronic states.

$TiO_2$ cell, the QD and the $TiO_2$ are negatively charged in the GS (−0.6 and −6.0 e, respectively), resulting in a $\mu_z$ of −15 D, which should slightly bend the $TiO_2$ CB edge toward lower energies. Upon photoexcitation, $\mu_z$ is reversed (+93 D), and the oxide unoccupied states raise.

To better understand the effect of the photoinduced shift of the oxide CB edge, we performed a series of calculations on the model shown in Figure 6a. In brief, we took the optimized geometry of the QD/CdS/$TiO_2$ system, and we removed the CdS layer. Then, we calculated the CSS of the QD/$TiO_2$ system for different QD−$TiO_2$ distances to check the effect of the positively charged QD in the negatively charged $TiO_2$ slabs. For comparison, we also calculated the corresponding oxidized (Ox) systems, which represent the effect of the hole residing in the QD on the neutral $TiO_2$ substrate. The CB edges calculated for the Ox systems are always less negative than those found for the CSS. Therefore, we performed a rigid shift of the CB of the former, in such a way that the first point (i.e., the smallest QD−$TiO_2$ distance) coincides with that calculated for the CSS, and set both values to zero. As it is evident from Figure 6b, for the cationic system, the CB edge raises with the increasing QD−$TiO_2$ distance because the electrostatic potential produced by the positively charged QD diminishes. Therefore, moving the positive charge away from the $TiO_2$ substrate is indeed beneficial for the functioning of the QDSSCs, in terms of the $V_{OC}$. A similar trend is found for the CSS. From our calculations, when the QD lies close to the $TiO_2$, there is no difference between the CSS and Ox states. With the increasing QD−$TiO_2$ distance, which experimentally corresponds to thickening the CdS layer, however, the CSS delivers a higher CB edge. Although the differences are quite small (due probably to the limitations of the model), they reveal an indubitable trend; in the QD/CdS/$TiO_2$ cells, there is an additional gain in $V_{OC}$, which adds to that due to displacing the positive charge apart from the oxide surface. The $\mu_z$ of the CSS increases monotonously with the QD−$TiO_2$ distance (see the Supporting Information), as it does the energy of the oxide CB edge. Precedent theoretical studies carried out by some of us on DSSCs demonstrate that the shift of the oxide CB edge correlates linearly with the electrostatic potential acting on the $TiO_2$ substrate.[22] The electrostatic potential due to a point charge varies as $1/r$ with the distance $r$ from the surface, whereas for the dipole, it changes with $1/r^2$. The shift of the CB calculated for our QD/$TiO_2$ (and the $V_{OC}$ measured experimentally for different thicknesses of the CDs layer)[29,30] fits none of these functional dependencies, suggesting that the improvement in PID cells is due in part to the interfacial dipole plus higher multipolar terms.

Summarizing, in this Letter, we have simulated the PID process in QDSSCs, which holds great potential in photovoltaics. We have demonstrated that the addition of type-II core/shell QDs to standard QDSSCs produces almost no changes on the GSs of the latter. Upon photoexcitation, however, the CB edge of the $TiO_2$ substrate experiences an additional shift, which in our model amounts to 25 meV. From our calculations, this shift is mainly due to displacing the photoexcited hole apart from the oxide surface, in such a way that the $TiO_2$ experiences a weaker electrostatic potential induced by the positive charge. However, the dipole (or higher multipolar electrostatic interactions) established between the newly injected electron and the hole residing in the QD core provides an additional gain in $V_{OC}$. We believe that this work, explaining the mechanisms by which PID cells deliver better efficiencies, paves the way for the design of new QDSSCs with improved efficiencies.

## COMPUTATIONAL DETAILS

All of the models have been fully optimized in the gas phase by means of the GGA-PBE[40] functional, in conjunction with the DZ basis set as implemented in the SIESTA 3.0 program package.[41] The inner electronic shells have been described through nonrelativistic pseudopotentials, whereas the H 1s, O 2s2p, S 3s3p, Ti and Zn 4s3d, Se 4s4p, and Cd 5s4d electrons have been explicitly included in the calculations. Although reliable for geometry optimizations, GGA functionals suffer from the well-known band gap underestimation problem.[42] To overcome this drawback, we have performed single-point calculations at the B3LYP[43]/3-21G* level on top of the PBE/DZ geometries, as implemented in the Gaussian09 software.[44] To properly describe the electronic structure of the models considered in this work, we have included the effect


DOI: 10.1021/acs.jpclett.5b00393
J. Phys. Chem. Lett. 2015, 6, 1423−1429

of the implicit solvent (water in this case, to reproduce the experiment) by means of the CPCM scheme.[45]

## ■ ASSOCIATED CONTENT

### Supporting Information

Dipole moments and charge displacement analysis (CDA). This material is available free of charge via the Internet at http://pubs.acs.org.

## ■ AUTHOR INFORMATION


### Corresponding Authors

*E-mail: jmkimteo@gmail.com ( J.M.A.).
*E-mail: filippo@thch.unipg.it (F.D.A.).


### Notes

The authors declare no competing financial interest.

## ■ ACKNOWLEDGMENTS

J.M.A. would like to thank Eusko Jaurlaritza (Basque Government) for funding through a postdoc fellowship.

## ■ REFERENCES


(1) Alivisatos, A. P. Semiconductor Clusters, Nanocrystals, and Quantum Dots. *Science* **1996**, *271*, 933−937.
(2) Murphy, C. J.; Coffer, J. L. Quantum Dots: A Primer. *Appl. Spectrosc.* **2002**, *56*, 16−27.
(3) Kamat, P. V. Quantum Dot Solar Cells. Semiconductor Nanocrystals as Light Harvesters. *J. Phys. Chem. C* **2008**, *112*, 18737−18753.
(4) Klimov, V. I. Mechanisms for Photogeneration and Recombination of Multiexcitons in Semiconductor. *J. Phys. Chem. B* **2006**, *110*, 16827−16845.
(5) Beard, M. C.; Midgett, A. G.; Hanna, M. C.; Luther, J. M.; Hughes, B. K.; Nozik, A. J. Comparing Multiple Exciton Generation in Quantum Dots to Impact Ionization in Bulk Semiconductors: Implications for Enhancement of Solar Energy Conversion. *Nano Lett.* **2010**, *10*, 3019−3027.
(6) Shockley, W.; Queisser, H. J. Detailed Balance Limit of Efficiency of p−n Junction Solar Cells. *J. Appl. Phys.* **1961**, *32*, 510−519.
(7) Hod, I.; Gonzalez-Pedro, V.; Tachan, Z.; Fabregat-Santiago, F.; Mora-Seró, I.; Bisquert, J.; Zaban, A. Dye versus Quantum Dots in Sensitized Solar Cells: Participation of Quantum Dot Absorber in the Recombination Process. *J. Phys. Chem. Lett.* **2011**, *2*, 3032−3035.
(8) Hod, I.; Zaban, A. Materials and Interfaces in Quantum Dot Sensitized Solar Cells: Challenges, Advances and Prospects. *Langmuir* **2014**, *30*, 7264−7273.
(9) Lee, H.; Leventis, H. C.; Moon, S.-J.; Chen, P.; Ito, S.; Haque, S. A.; Torres, T.; Nüesch, F.; Geiger, T.; Zakeeruddin, S. M.; Grätzel, M.; Nazeeruddin, M. K. PbS and CdS Quantum Dot-Sensitized Solid-State Solar Cells: "Old Concepts, New Results". *Adv. Funct. Mater.* **2009**, *19*, 2735−2742.
(10) Rühle, S.; Shalom, M.; Zaban, A. Quantum-Dot-Sensitized Solar Cells. *ChemPhysChem* **2010**, *11*, 2290−304.
(11) O'Regan, B.; Grätzel, M. A Low-Cost, High-Efficiency Solar Cell Based on Dye-Sensitized Colloidal $TiO_2$ Films. *Nature* **1991**, *353*, 737−740.
(12) Jiao, S.; Shen, Q.; Mora-Seró, I.; Wang, J.; Pan, Z.; Zhao, K.; Kuga, Y.; Zhong, X.; Bisquert, J. Band Engineering in Core/Shell ZnTe/CdSe for Photovoltage and Efficiency Enhancement in Exciplex. *ACS Nano* **2015**, 908−915.
(13) Mathew, S.; Yella, A.; Gao, P.; Humphry-Baker, R.; Curchod, B. F. E.; Ashari-Astani, N.; Tavernelli, I.; Rothlisberger, U.; Nazeeruddin, M. K.; Grätzel, M. Dye-Sensitized Solar Cells with 13% Efficiency Achieved through the Molecular Engineering of Porphyrin Sensitizers. *Nat. Chem.* **2014**, *6*, 242−247.
(14) Jeon, N. J.; Noh, J. H.; Yang, W. S.; Kim, Y. C.; Ryu, S.; Seo, J.; Seok, S. I. Compositional Engineering of Perovskite Materials for High-Performance Solar Cells. *Nature* **2015**, *517*, 476−480.
(15) Zhou, H.; Chen, Q.; Li, G.; Luo, S.; Song, T.-b.; Duan, H.-S.; Hong, Z.; You, J.; Liu, Y.; Yang, Y. Interface Engineering of Highly Efficient Perovskite Solar Cells. *Science* **2013**, *345*, 542−546.
(16) Fan, J.; Hao, Y.; Cabot, A.; Johansson, E. M. J.; Boschloo, G.; Hagfeldt, A. Cobalt(II/III) Redox Electrolyte in ZnO Nanowire-Based Dye-Sensitized Solar Cells. *ACS Appl. Mater. Interfaces* **2013**, *5*, 1902−1906.
(17) Lim, C.-S.; Im, S. H.; Rhee, J. H.; Lee, Y. H.; Kim, H.-J.; Maiti, N.; Kang, Y.; Chang, J. A.; Nazeeruddin, M. K.; Grätzel, M.; Seok, S. I. Hole-Conducting Mediator for Stable $Sb_2S_3$-Sensitized Photoelectrochemical Solar Cells. *J. Mater. Chem.* **2012**, *22*, 1107−1111.
(18) Fantacci, S.; De Angelis, F.; Nazeeruddin, M. K.; Gr, M. Electronic and Optical Properties of the Spiro-MeOTAD Hole Conductor in Its Neutral and Oxidized Forms: A DFT/TDDFT Investigation. *J. Phys. Chem. C* **2011**, *115*, 23126−23133.
(19) Chang, J. A.; Im, S. H.; Lee, Y. H.; Kim, H.-J.; Lim, C.-S.; Heo, J. H.; Seok, S. I. Panchromatic Photon-Harvesting by Hole-Conducting Materials in Inorganic−Organic Heterojunction Sensitized-Solar Cell through the Formation of Banostructured Electron Channels. *Nano Lett.* **2012**, *12*, 1863−1867.
(20) Chang, J. A.; Rhee, J. H.; Im, S. H.; Lee, Y. H.; Kim, H.-j.; Seok, S. I.; Nazeeruddin, M. K.; Gratzel, M. High-Performance Nanostructured Inorganic-Organic Heterojunction Solar Cells. *Nano Lett.* **2010**, *10*, 2609−2612.
(21) Im, S. H.; Lim, C.-S.; Chang, J. A.; Lee, Y. H.; Maiti, N.; Kim, H.-J.; Nazeeruddin, M. K.; Grätzel, M.; Seok, S. I. Toward Interaction of Sensitizer and Functional Moieties in Hole-Transporting Materials for Efficient Semiconductor-Sensitized Solar Cells. *Nano Lett.* **2011**, *11*, 4789−4793.
(22) Ronca, E.; Pastore, M.; Belpassi, L.; Tarantelli, F.; De Angelis, F. Influence of the Dye Molecular Structure on the $TiO_2$ Conduction Band in Dye-Sensitized Solar Cells: Disentangling Charge Transfer and Electrostatic Effects. *Energy Environ. Sci.* **2013**, *6*, 183−193.
(23) Rühle, S.; Greenshtein, M.; Chen, S.-G.; Merson, A.; Pizem, H.; Sukenik, C. S.; Cahen, D.; Zaban, A. Molecular Adjustment of the Electronic Properties of Nanoporous Electrodes in Dye-Sensitized Solar Cells. *J. Phys. Chem. B* **2005**, *109*, 18907−18913.
(24) Zaban, A.; Bisquert, J.; Ilan, B.; Uni, V.; Gan, R. Design of Injection and Recombination in Quantum Dot Sensitized Solar Cells. *J. Am. Chem. Soc.* **2010**, 6834−6839.
(25) Shalom, M.; Rühle, S.; Hod, I.; Yahav, S.; Zaban, A. Energy Level Alignment in CdS Quantum Dot Sensitized Solar Cells Using Molecular Dipoles. *J. Am. Chem. Soc.* **2009**, *131*, 9876−9877.
(26) Hod, I.; Tachan, Z.; Shalom, M.; Zaban, A. Characterization and Control of the Electronic Properties of a NiO Based Dye Sensitized Photocathode. *Phys. Chem. Chem. Phys.* **2013**, *15*, 6339−6343.
(27) Shalom, M.; Tachan, Z.; Bouhadana, Y.; Barad, H.-N.; Zaban, A. Illumination Intensity-Dependent Electronic Properties in Quantum Dot Sensitized Solar Cells. *J. Phys. Chem. Lett.* **2011**, *2011*, 1998−2003.
(28) Shalom, M.; Buhbut, S.; Tirosh, S.; Zaban, A. Design Rules for High-Efficiency Quantum-Dot-Sensitized Solar Cells: A Multilayer Approach. *J. Phys. Chem. Lett.* **2012**, *3*, 2436−2441.
(29) Kazes, M.; Buhbut, S.; Itzhakov, S.; Lahad, O.; Zaban, A.; Oron, D. Photophysics of Voltage Increase by Photoinduced Dipole Layers in Sensitized Solar Cells. *J. Phys. Chem. Lett.* **2014**, *5*, 2717−2722.
(30) Buhbut, S.; Itzhakov, S.; Hod, I.; Oron, D.; Zaban, A. Photo-Induced Dipoles: A New Method to Convert Photons into Photovoltage in Quantum Dot Sensitized Solar Cells. *Nano Lett.* **2013**, *13*, 4456−4461.
(31) De Angelis, F.; Fantacci, S.; Mosconi, E.; Nazeeruddin, M. K.; Gr, M. Absorption Spectra and Excited State Energy Levels of the N719 Dye on $TiO_2$ in Dye-Sensitized Solar Cell Models. *J. Phys. Chem. C* **2011**, *115*, 8825−8831.
(32) Grätzel, M. Photoelectrochemical Cells. *Nature* **2001**, *414*, 338−344.




DOI: 10.1021/acs.jpclett.5b00393
*J. Phys. Chem. Lett.* 2015, 6, 1423−1429

(33) Yin, L.-W.; Bando, Y.; Zhan, J.-H.; Li, M.-S.; Golberg, D. Self-Assembled Highly Faceted Wurtzite-Type ZnS Single-Crystalline Nanotubes with Hexagonal Cross-Sections. *Adv. Mater.* **2005**, *17*, 1972−1977.
(34) Azpiroz, J. M.; Infante, I.; Lopez, X.; Ugalde, J. M.; De Angelis, F. A First-Principles Study of II−VI (II = Zn; VI = O, S, Se, Te) Semiconductor Nanostructures. *J. Mater. Chem.* **2012**, *22*, 21453−21465.
(35) Azpiroz, J. M.; Mosconi, E.; De Angelis, F. Modeling ZnS and ZnO Nanostructures: Structural, Electronic, and Optical Properties. *J. Phys. Chem. C* **2011**, *115*, 25219−25226.
(36) Qi, L.; Cölfen, H.; Antonietti, M. Synthesis and Characterization of CdS Nanoparticles Stabilized by Double-Hydrophilic Block Copolymers. *Nano Lett.* **2001**, *1*, 61−65.
(37) Spanó, E.; Hamad, S.; Catlow, C. R. A. ZnS Bubble Clusters with Onion-Like Structures. *Chem. Commun.* **2004**, *7*, 864−865.
(38) Mora-Seró, I.; Bisquert, J. Breakthroughs in the Development of Semiconductor-Sensitized Solar Cells. *J. Phys. Chem. Lett.* **2010**, *1*, 3046−3052.
(39) Azpiroz, J. M.; Ugalde, J. M.; Etgar, L.; Infante, I.; De Angelis, F. The Effect of $TiO_2$ Morphology on the Electron Injection Efficiency in PbS Quantum Dot Solar Cells: A First-Principles Study. *Phys. Chem. Chem. Phys.* **2015**, *17*, 6076−6086.
(40) Perdew, J. P.; Burke, K.; Ernzerhof, M. Generalized Gradient Approximation Made Simple. *Phys. Rev. Lett.* **1996**, *77*, 3865−3868.
(41) Soler, J. M.; Artacho, E.; Gale, J. D.; García, A.; Junquera, J.; Ordejón, P.; Sánchez-Portal, D. The SIESTA Method for Ab Initio Order-N Materials Simulation. *J. Phys.: Condens. Matter* **2002**, *14*, 2745−2779.
(42) Azpiroz, J. M.; Ugalde, J. M.; Infante, I. Benchmark Assessment of Density Functional Methods on Group II−VI MX (M = Zn, Cd; X = S, Se, Te) Quantum Dots. *J. Chem. Theory Comput.* **2014**, *10*, 76−89.
(43) Becke, A. D. A New Mixing of Hartree−Fock and Local Density-Functional Theories. *J. Chem. Phys.* **1993**, *98*, 1372−1377.
(44) Frisch, M. J.; Trucks, G. W.; Schlegel, H. B.; Scuseria, G. E.; Robb, M. A.; Cheeseman, J. R.; Scalmani, G.; Barone, V.; Mennucci, B.; Petersson, G. A.; et al. *Gaussian 09*, revision B.01; Gaussian Inc.: Wallingford, CT, 2009.
(45) Cossi, M.; Rega, N.; Scalmani, G.; Barone, V. Energies, Structures, and Electronic Properties of Molecules in Solution with the C-PCM Solvation Model. *J. Comput. Chem.* **2003**, *24*, 669−681.


DOI: 10.1021/acs.jpclett.5b00393
*J. Phys. Chem. Lett.* 2015, 6, 1423−1429